Mechanics of Advanced Composite Structures

Journal homepage: https://macs.semnan.ac.ir/

Semnan University

ISSN: 2423-7043

Research Article

Large Deformation Elastic Analysis of Pressurized FGM Thick Cylindrical Shells with Nonlinear Plane Elasticity Theory (NPET)

Navid Bahadorani, Mehdi Ghannad *, Mohammad-Hossein Sohani , Bahman Modiri

Department of Mechanical Engineering, Shahrood University of Technology, Shahrood, Iran

ARTICLE INFO

Article history:

Received: 2024-03-03

Revised: 2024-06-30

Accepted: 2024-07-21

Keywords:

Pressurized cylinder;

Large deformation;

Nonlinear plane elasticity theory;

Perturbation technique;

Functionally graded materials.

ABSTRACT

In the present study, the governing equation of pressurized axisymmetric thick cylinders made of Functionally Graded materials (FGMs) with large deformations is derived using the Nonlinear Plane Elasticity Theory (NPET). Because of large deformations along the radial direction and hence the existence of nonlinear terms in kinematic equations, the governing equation is a nonlinear second-order equation with variable coefficients, which is solved in plane stress and plane strain states using the perturbation technique. According to the equilibrium equation, boundary conditions and different end conditions of the cylinder: open ends and closed ends; radial, axial, and circumferential stresses and radial displacement in cylindrical shells are analytically calculated. To investigate the accuracy of the results obtained from the analytical solution, the numerical finite element modeling of the mentioned cylinder with ABAQUS software based on the nonlinear elasticity theory is done and the results of the two methods are compared. This research reveals that the obtained results by the mentioned analytical solution procedure have good accuracy for cylindrical shells under pressure load. The aim of this study is to provide a mathematical solution for the nonlinear analysis of large deformations of FGM cylinders.

1. Introduction

In mechanical science, Functionally Graded Materials (FGMs) may be characterized by the variation in composition and structure gradually over volume, resulting in corresponding changes in the properties of the material. FGMs are advanced materials with gradient compositional variation of two or more materials that are varied continuously as a function of position along certain dimensions of the structure. The FGM's are adequate for many industrial departments such as corrosion and erosion-resistant coatings, dental implants, heat exchanger conduits, heat diffuser plates, plasma coatings for nuclear fusion, etc.

Lamé provided an exact solution for isotropic axisymmetric thick-walled cylinders, his solution later led to Plane Elasticity Theory (PET) [1]. Zhifei et al. reported the exact solution of FGM hollow cylinders with isotropic multilayers based on Lamé's solution [2]. Sanders indicated strain-displacement relations for thin shells while considering the large deformations, he simplified the equilibrium and strain-displacement relationships using assumptions [3]. Fukui and Yamanaka extracted and solved the governing equation of a thick-walled FGM pipe under

*** Corresponding author.**
E-mail address: *mghannadk@shahroodut.ac.ir & ghannad.mehdi@gmail.com*

Cite this article as:

Bahadorani, N., Ghannad, M., Sohani, M. H. and Modiri, B., 2025. Large Deformation Elastic Analysis of Pressurized FGM Thick Cylindrical Shells with Nonlinear Plane Elasticity Theory (NPET). *Mechanics of Advanced Composite Structures*, 12(1), pp. 129-140.

https://doi.org/10.22075/MACS.2024.33431.1619

internal pressure using the classical theory (PET) and the Runge-Kutta numerical method [4]. Thomas and Liu analyzed the large strain and large rotation of the shells and finally arrived at a nonlinear finite element formulation [5]. By considering a power function for Young's modulus, Ghannad and Nejad analyzed thick-walled cylindrical shells under internal and external pressure using PET [6]. In the same year, Ghannad and Gharooni analyzed symmetric thick-walled cylinders made of performance-graded materials under uniform internal and external pressure using High-order Shear Deformation Theory (HSDT) instead of PET [7]. Ghannad and Nejad derived an analytical formula based on the First-order Shear Deformation Theory (FSDT) for axisymmetric thick-walled inhomogeneous cylinders under uniform internal and external pressure considering a power function for FGMs [8]. The next year, they derived the governing equations of thick cylindrical shells with variable thickness made of FGMs with clamped-clamped end conditions. They solved the equations analytically using the Matched Asymptotic Method (MAM) of the perturbation technique [9]. Tang and Bich investigated the nonlinear response of the spherical shell, assuming that the variation of mechanical properties along the radius of the sphere follows a power function. In this research, temperature effects were considered in addition to pressure effects [10]. Static and dynamic nonlinear stability of functionally graded plates and shells was investigated by Duc [11]. Thuy Anh et al. studied thin annular Functionally Graded spherical shells too, but they investigated the stability of these shells under external pressure and temperature [12]. Ranjen Kar and Kumar Panda examined the linear and nonlinear deformation behavior of the FGM spherical shell panel under thermomechanical load. The nonlinear mathematical model of the FG shell panel was developed based on HSDT and green Lagrange-type geometrical nonlinearity [13]. Srividhya et al. carried out a nonlocal nonlinear analysis of functionally graded plates subjected to static loads based on the Third-order Shear Deformation Theory (TSDT) and von Karman nonlinear strains [14]. Sofiyev and Dikmen studied the buckling of shells composed of FGM under uniform compressive lateral pressure, they did this for mixed boundary conditions [15]. Quan et al. studied the nonlinear vibration of porous functionally graded sandwich plates on elastic foundations based on the Reddy high-order shear deformation theory of von Kármán type nonlinearity, they employed Reddy's higher-order shear deformation theory [16]. Bahadorani et al. derived a governing equation of pressurized axisymmetric cylinders made of homogeneous and isotropic materials with large deformations and small strains using NPET [17]. Ellouz et al. inspect the magneto-electro-elastic coupling performance of thin-walled smart structures with laminate design presenting FGM composite using improved first-order shear deformation, they proposed a new useful MEE FE model [18].

Previous research generally relied on numerical or semi-analytical methods, while this article is done using a mathematical and analytical method purely. The perturbation technique is a mathematical method for solving nonlinear differential equations. Of course, if shear stress and strain appear in the problem, this method is not solved. In the present paper, the governing equation of pressurized thick-walled axisymmetric thick cylindrical shells made of Functionally Graded materials (FGMs) with large deformations and small strains is derived using Nonlinear Plane Elasticity Theory (NPET). The governing equation is solved in plane stress and plane strain states using the perturbation technique. The application of this research is for non-hyper elastic materials that follow Hooke's law and do not have extremely small deformations (they have large deformations relatively).

2. Formulation

Linear constitutive equations (Hook's low) are used in the extraction of governing equations. The shell material is assumed to be functionally graded along the radius. The cylinder thickness is constant and it is subjected to uniform pressure in internal and/or external radii. The problem is considered to be completely axisymmetric. Figure 1 shows the cross-section of the thick cylinder under study.

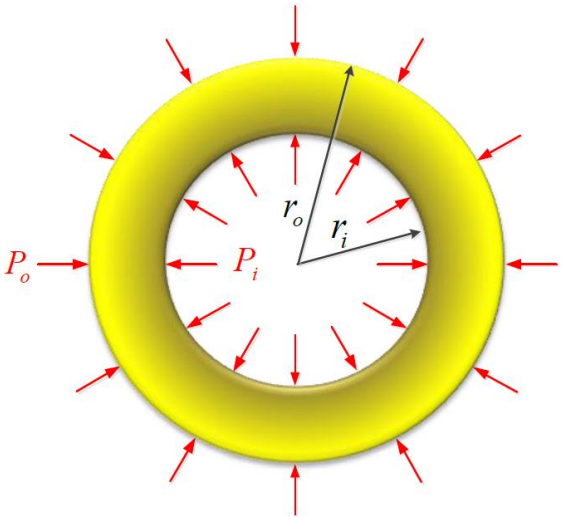

Fig. 1. Cross section of cylindrical shell

Similar to Plane Elasticity Theory (PET), in Nonlinear Plane Elasticity Theory (NPET), it is

assumed that sections that are planar and perpendicular to the central axis of the cylinder, remain in the same position after deformations due to pressure loadings. In other words, the shear effect is ignored. In addition, stress and strain tensors will be diagonal. Thus, radial and axial deformations are dependent only on radial and axial coordinates, respectively.

The axisymmetric equilibrium equations in the cylindrical coordinate system and the absence of body forces are expressed as:

$$div\tilde{\sigma} = 0 \begin{cases} \sigma_{r,r} + \frac{1}{r}(\sigma_r - \sigma_\theta) = 0 \\ \sigma_{x,x} = 0 \end{cases} \quad (1)$$

where σ_r, σ_θ and σ_x are radial, circumferential, and axial stresses, respectively. The nonlinear kinematic equation in general is as follows.

$$\tilde{\varepsilon} = \frac{1}{2}\left[(\vec{\nabla}\vec{u}) + (\vec{\nabla}\vec{u})^T + (\vec{\nabla}\vec{u})^T(\vec{\nabla}\vec{u})\right] \quad (2)$$

According to assumptions, the problem is completely axisymmetric (geometry, material, and loading) and large deformation occurs only along the radial direction. Therefore general strain-displacement relations (2) reduce to the following form (Saint Venant-Kirchhoff model).

$$\begin{cases} \varepsilon_r = u_{r,r} + \frac{1}{2}(u_{r,r})^2 \\ \qquad \vdots \\ \varepsilon_\theta = \frac{1}{r}u_r + \frac{1}{2}\left(\frac{1}{r}u_r\right)^2 \\ \qquad \vdots \\ \varepsilon_x = u_{x,x} \end{cases} \quad (3)$$

where ε_r, ε_θ and ε_x denote radial, circumferential, axial strains; u_r and u_x radial and axial displacements, respectively. A comma in subscript denotes derivative concerning the variable written just after it. The constitutive relations for nonhomogeneous and isotropic materials are [6]:

$$\begin{Bmatrix} \sigma_r \\ \sigma_\theta \end{Bmatrix} = E(r)\begin{bmatrix} A & B \\ B & A \end{bmatrix}\begin{Bmatrix} \varepsilon_r \\ \varepsilon_\theta \end{Bmatrix} \quad (4)$$
$$\sigma_x = \alpha(\sigma_r + \sigma_\theta)$$

where $E(r)$ is Young's modulus and A and B are constants related to Poisson's ratio ν as described below.

I). Plane stress (cylinder with open ends) [6]

$$\sigma_x = 0 \ , \ \varepsilon_x \neq 0 \ , \ \alpha = 0$$
$$A = \frac{1}{1-\nu^2} \ , \ B = \frac{\nu}{1-\nu^2} \ , \ \nu^* = \frac{B}{A} = \nu \quad (5)$$

II). Plane strain (cylinder with closed ends) [6]

$$\sigma_x \neq 0 \ , \ \varepsilon_x = 0 \ , \ \alpha = \nu$$
$$A = \frac{1-\nu}{(1+\nu)(1-2\nu)}, \quad (6)$$
$$B = \frac{\nu}{(1+\nu)(1-2\nu)} \ , \ \nu^* = \frac{B}{A} = \frac{\nu}{1-\nu}$$

where α is dependent on end conditions. As a common assumption, the Poisson's ratio is considered to be constant, because of the minor effects its change has on analysis results. The nonhomogeneous Young's modulus $E(r)$ is the power function of dimensionless radial coordinate $\bar{r}$.

$$E(r) = E_i\bar{r}^n \quad (7)$$

In (7), E_i is the modulus of elasticity at the inner surface (i.e. surface at $r = r_i$) and n is the inhomogeneity constant, determined empirically and the radial coordinate (r) is normalized as $\bar{r} = r/r_i$.

By substituting (3) and (7) into (4) and the use of (1), and after some simplifications, one may lead to the following equation.

$$[E(r)(A\varepsilon_r + B\varepsilon_\theta)]_{,r} + \frac{1}{r}[E(r)(A-B)(\varepsilon_r - \varepsilon_\theta)] = 0 \quad (8)$$

$$\begin{aligned} &Au_{r,rr} + \frac{A(n+1)}{r}u_{r,r} + \frac{(Bn-A)}{r^2}u_r \\ &+ Au_{r,r}u_{r,rr} + \frac{B}{r^2}u_r u_{r,r} \\ &+ \frac{(An+A-B)}{2r}(u_{r,r})^2 \\ &+ \frac{(Bn-B-A)}{2r^3}u_r^2 = 0 \end{aligned} \quad (9)$$

Equation (9) is the governing equation of the NPET problem.

3. Solution

The first step for solving NPET equation (9) is to make it dimensionless using the dimensionless parameters that are listed in appendix.

$$\begin{aligned} &A\left[u^*_{r,r^*r^*} + \frac{(n+1)}{r^*}u^*_{r,r^*} + \frac{(\nu^*n-1)}{r^{*2}}u^*_r\right] \\ &+\left[\left(u^*_{r,r^*}u^*_{r,r^*r^*}\right) + \left(\nu^* u^*_r \frac{u^*_{r,r^*}}{r^{*2}}\right)\right. \\ &\qquad + \frac{(n+1-\nu^*)}{2r^*}\left(u^*_{r,r^*}\right)^2 \\ &\qquad \left. + \frac{(\nu^*n-\nu^*-1)}{2r^{*3}}u_r^{*2}\right]\epsilon \\ &\qquad = 0 \end{aligned} \quad (10)$$

Compared to lower-order derivatives, higher-order derivatives are not dominant; thus the (10) mathematically represents a regular perturbation problem. So, the dimensionless radial displacement can be expanded as follows.

$$u_r^* = u_0 + \epsilon u_1 + O(\epsilon^2) \tag{11}$$

The term $O(\epsilon^2)$ is a term of ϵ^2 magnitude. By substituting (11) into (10) and then separating the coefficients of the same powers of perturbation parameter ϵ, the equation can be rewritten as follows.

$$\begin{aligned}&\left(u_{0,r^*r^*} + (n+1)\frac{u_{0,r^*}}{r^*} + (\nu^* n - 1)\frac{u_0}{r^{*2}}\right)\frac{\epsilon^0}{R} \\ &+ \left(\left(u_{1,r^*r^*} + \frac{(n+1)u_{1,r^*}}{r^*} + \frac{(\nu^* n - 1)u_1}{r^{*2}}\right) + \left(u_{0,r^*}\, u_{0,r^*r^*}\right) + \left(\nu^* \frac{u_0 u_{0,r^*}}{r^{*2}}\right) + \frac{(n+1-\nu^*)}{2r^*}\left(u_{0,r^*}\right)^2 + \frac{(\nu^* n - \nu^* - 1)}{2r^{*3}}u_0^2\right)\frac{\epsilon^1}{R} + O(\epsilon^2) = 0\end{aligned} \tag{12}$$

For $\epsilon \ll 1$, (12) is held only when the coefficients of different powers of epsilon are zero.

3.1. Zero-Order Equation (Coefficient of ϵ^0)

In this case, equation (ϵ^0 coefficients) is expressed as:

$$u_{0,r^*r^*} + (n+1)\frac{u_{0,r^*}}{r^*} + (\nu^* n - 1)\frac{u_0}{r^{*2}} = 0 \tag{13}$$

which is a linear ordinary differential equation with variable coefficients. To solve (13) one can substitute $u_0(r^*) = r^{*^t}$ into it. This leads to the characteristic equation below.

$$t^2 + nt + (\nu^* n - 1) = 0 \tag{14}$$

The roots of the characteristic equation are:

$$t_1, t_2 = \frac{-n \pm \sqrt{\Delta}}{2}, \Delta = n^2 - 4(\nu^* n - 1) \tag{15}$$

These roots are real, because $\Delta > 0$ consistently holds. So the solution of (14) is a linear combination of terms corresponding to each of the two roots (15).

$$u_0 = C_1 r^{*t_1} + C_2 r^{*t_2} \tag{16}$$

where C_1 and C_2 are constants to be determined later.

3.2. First-Order Equation (Coefficient of ϵ^1)

The next equation to be solved is the ϵ^1 coefficient.

$$\begin{aligned}&\left(u_{1,r^*r^*} + \frac{(n+1)u_{1,r^*}}{r^*} + \frac{(\nu^* n - 1)u_1}{r^{*2}}\right) + \left(u_{0,r^*}\, u_{0,r^*r^*}\right) + \left(\nu^* \frac{u_0 u_{0,r^*}}{r^{*2}}\right) \\ &+ \frac{(n+1-\nu^*)}{2r^*}\left(u_{0,r^*}\right)^2 + \frac{(\nu^* n - \nu^* - 1)}{2r^{*3}}u_0^2 = 0\end{aligned} \tag{17}$$

When a zero-order solution is obtained, by substituting that into (17), a second-order linear nonhomogeneous differential equation is obtained.

$$\begin{aligned}&u_{1,r^*r^*}r^{*2} + (n+1)u_{1,r^*}r^* + (\nu^* n - 1)u_1 \\ &= -\left[t_1^3 + \nu^* t_1 + \frac{n-1-\nu^*}{2}t_1^2 + \frac{\nu^* n - \nu^* - 1}{2}\right]C_1^2 r^{*(2t_1-1)} \\ &- \left[t_2^3 + \nu^* t_2 + \frac{n-1-\nu^*}{2}t_2^2 + \frac{\nu^* n - \nu^* - 1}{2}\right]C_2^2 r^{*(2t_2-1)} \\ &- [(t_1+t_2)t_1 t_2 + \nu^*(t_1+t_2) + (n-1-\nu^*)t_1 t_2 + (\nu^* n - \nu^* - 1)]C_1 C_2 r^{*(t_1+t_2-1)}\end{aligned} \tag{18}$$

Equation (18) has a homogeneous solution (u_{1h}) and a particular solution (u_{1p}). The homogeneous form of (18) is the same as the zero-order equation (13). Therefore the u_{1h} has a similar solution with the same roots for characteristic equation t_1 and t_2.

$$u_{1h} = C_3 r^{*t_1} + C_4 r^{*t_2} \tag{19}$$

Using the Wronskian method in (18), the particular solution can be obtained as follows.

$$\begin{aligned}u_{1p} &= \left(\frac{1}{(2t_1 - t_2 + 1)} - \frac{1}{(t_1+1)}\right)\frac{K_1}{(t_2 - t_1)}r^{*(2t_1+1)} \\ &+ \left(\frac{1}{(t_2+1)} - \frac{1}{(2t_2 - t_1 + 1)}\right)\frac{K_2}{(t_2 - t_1)}r^{*(2t_2+1)} \\ &+ \left(\frac{1}{(t_1+1)} - \frac{1}{(t_2+1)}\right)\frac{K_3}{(t_2 - t_1)}r^{*(t_1+t_2+1)}\end{aligned} \tag{20}$$

In which:

$$K_1 = -\left[t_1^3 + \nu^* t_1 + \frac{n-1-\nu^*}{2} t_1^2 + \frac{\nu^* n - \nu^* - 1}{2}\right] C_1^2$$

$$K_2 = -\left[t_2^3 + \nu^* t_2 + \frac{n-1-\nu^*}{2} t_2^2 + \frac{\nu^* n - \nu^* - 1}{2}\right] C_2^2 \quad (21)$$

$$K_3 = -[(t_1+t_2)t_1 t_2 + \nu^*(t_1+t_2) + (n-1-\nu^*)t_1 t_2 + (\nu^* n - \nu^* - 1)]C_1 C_2$$

So, the general solution of (18) will be the sum of the homogeneous and the particular solution;

$$u_1 = u_{1h} + u_{1p} \quad (22)$$

Now, dimensionless radial displacement can be approximated according to (11).

$$\begin{aligned} u_r^* &\cong (C_1 + \epsilon C_3) r^{*t_1} + (C_2 + \epsilon C_4) r^{*t_2} \\ &+ \epsilon \left[\left(\frac{1}{(2t_1 - t_2 + 1)} - \frac{1}{(t_1+1)} \right) \frac{K_1}{(t_2 - t_1)} r^{*(2t_1+1)} \right. \\ &+ \left(\frac{1}{(t_2+1)} - \frac{1}{(2t_2 - t_1 + 1)} \right) \frac{K_2}{(t_2 - t_1)} r^{*(2t_2+1)} \\ &\left. + \left(\frac{1}{(t_1+1)} - \frac{1}{(t_2+1)} \right) \frac{K_3}{(t_2 - t_1)} r^{*(t_1+t_2+1)} \right] \end{aligned} \quad (23)$$

Using dimensionless parameters (A1) and substituting (23) into (2) and making use of (3), dimensionless radial stress can be obtained. To determine the unknown constants C_1, C_2, C_3 and C_4, the boundary conditions should be applied. To this end, the dimensionless form of boundary conditions for internal and external pressure loading is used.

$$\sigma_r^* \big|_{r^* = r_i^*} = -P_i^*$$
$$\sigma_r^* \big|_{r^* = r_o^*} = -P_o^* \quad (24)$$

Substituting (24) into (A2), leads to two algebraic equations including different powers of ϵ. Again, as the perturbation parameter is too small compared to unity, different powers of ϵ on both sides of the equation should be equal. It gives required equations for the calculation of the unknown constants, whose final results are listed in appendix equations (A3) to (A6).

4. Case Study and Results Survey

In this section, firstly, the nonlinear response is investigated within a case study. In the following, the effects of different parameters on nonlinear behavior are shown. To verify the validity of the presented analytical solution method, the results of the NPET and FEM are presented in section 4.2.

4.1. Case Study

Consider a nonhomogeneous cylinder with constant thickness, inner radius $r_i = 30$ mm, outer radius $r_o = 34$ mm, length $L = 400$ mm and power distribution of modulus of elasticity. The modulus of elasticity E_i at the internal radius has the value of 0.7 GPa. It is also assumed that the passion's ratio ν has a constant value of 0.3. The cylinder is subjected to internal and external pressures $P_i = 8$ MPa, and $P_o = 8$ MPa, respectively. For this cylinder, the plane strain condition is used. In Figures 2 to 6, the distribution of stresses and radial displacement through the wall thickness for different values of n are plotted.

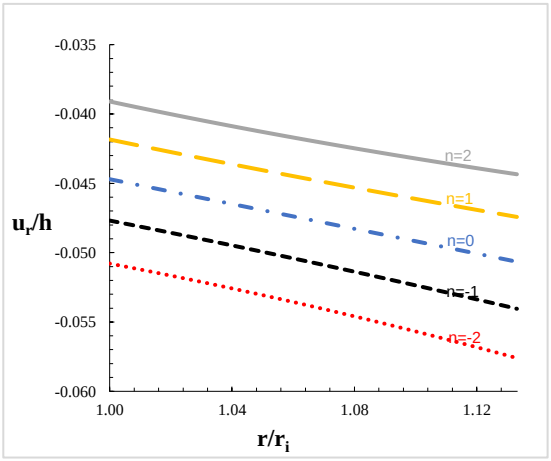

Fig. 2. Distribution of dimensionless radial displacement in plane strain state, $P_i = P_o = 8$ MPa

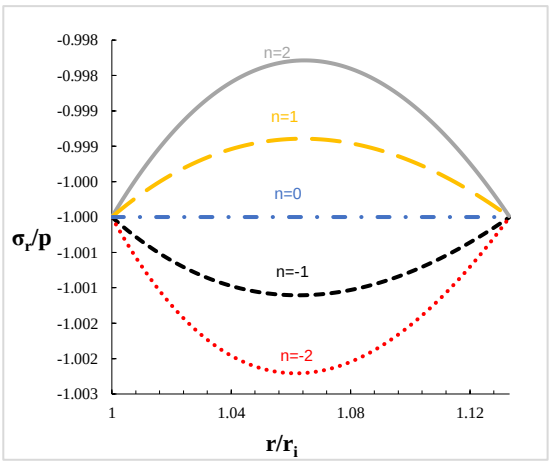

Fig. 3. Distribution of dimensionless radial stress in plane strain state, $P_i = P_o = 8$ MPa

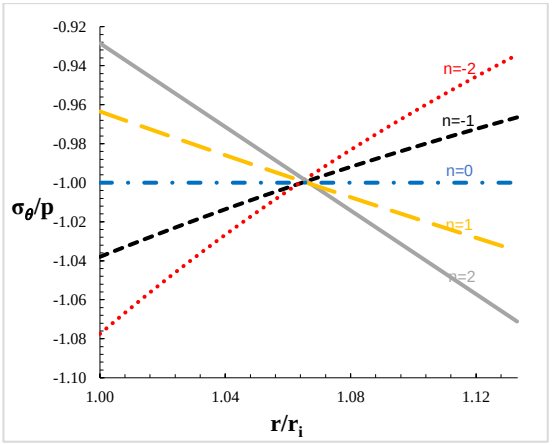

Fig. 4. Distribution of dimensionless circumferential stress in plane strain state, $P_i = P_o = 8$ MPa

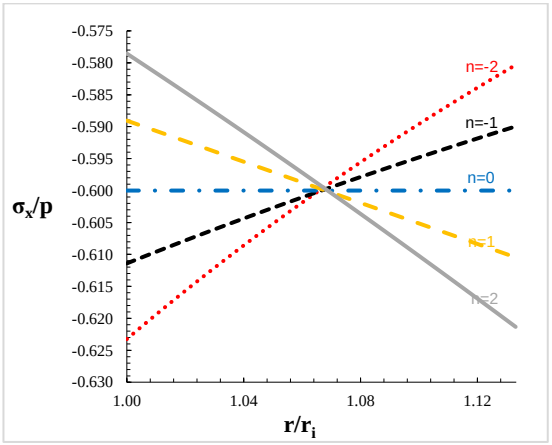

Fig. 5. Distribution of dimensionless axial stress in plane strain state, $P_i = P_o = 8$ MPa

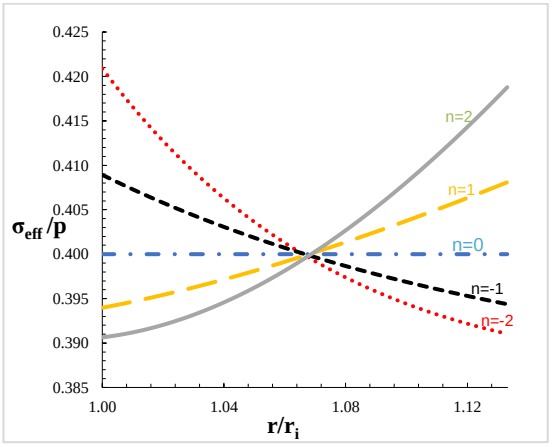

Fig. 6. Distribution of von Mises effective stress in plane strain state, $P_i = P_o = 8$ MPa

We know, uniform internal and external pressure cause positive and negative displacement respectively. As seen in Figures 2 and 3, displacement and radial stress have negative values. Since the cylinder is under uniform internal and external pressure, because of greater influence of the stress caused by external pressure than internal pressure, the external pressure has dominant effect and causes negative displacement. It can also be seen in Figures 4 and 5 that heterogeneous materials with positive constant values of heterogeneity cause a decrease in circumferential and axial stresses along the radius of the cylinder, while negative constant values of heterogeneity increase the stresses along the radius direction.

4.2. Effective Parameters on Nonlinear Response

4.2.1. Effects of End Conditions

In this section, the distribution of stresses and radial displacement is compared with the solution from reference [1]. The cylinder is only under internal pressure, $P_i = 8$ MPa. It is also assumed that $E = 0.7$ GPa and the shell is homogeneous ($n = 0$). Distribution of radial displacement, radial stress, circumferential stress and axial stress are shown for plane stress and plane strain conditions, in Figures 7 to 10, respectively.

Figure 7 shows that radial displacement in plane stress state has higher values than plane strain in all three types of loadings (internal pressure, external pressure and internal and external pressure), while the boundary conditions do not have much effect on the radial and circumferential stress (see Figures 8 to 10).

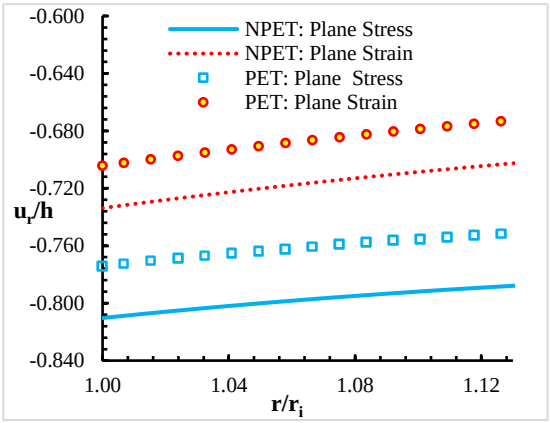

Fig. 7. Distribution of dimensionless radial displacement calculated by NPET and PET, $P_i = 8$ MPa (homogeneous cylinder)

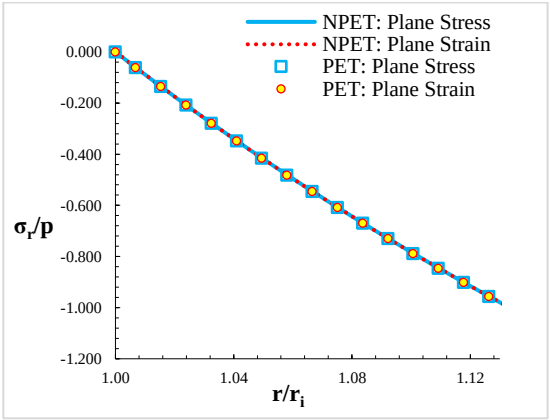

Fig. 8. Distribution of dimensionless radial stress calculated by NPET and PET, $P_i = 8$ MPa (homogeneous cylinder)

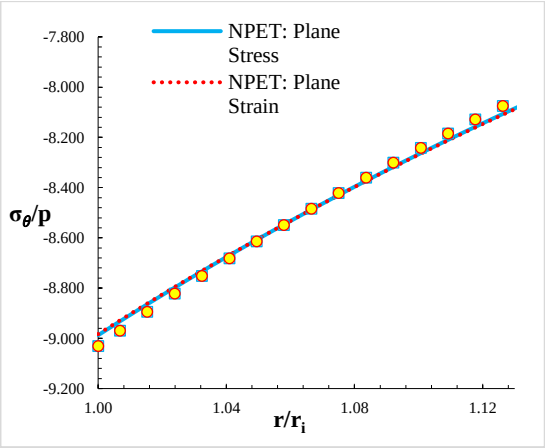

Fig. 9. Distribution of dimensionless circumferential stress calculated by NPET and PET, $P_i = 8$ MPa (homogeneous cylinder)

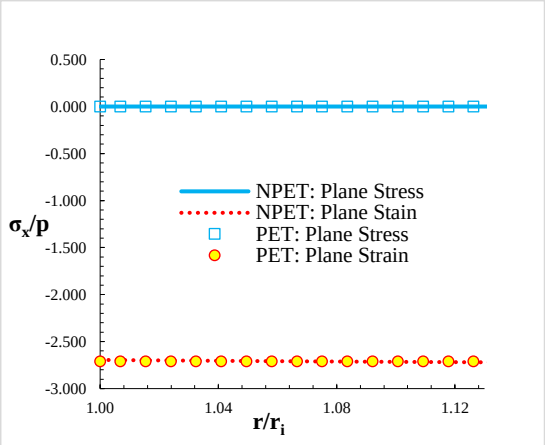

Fig. 10. Distribution of dimensionless axial stress calculated by NPET and PET, $P_i = 8$ MPa (homogeneous cylinder)

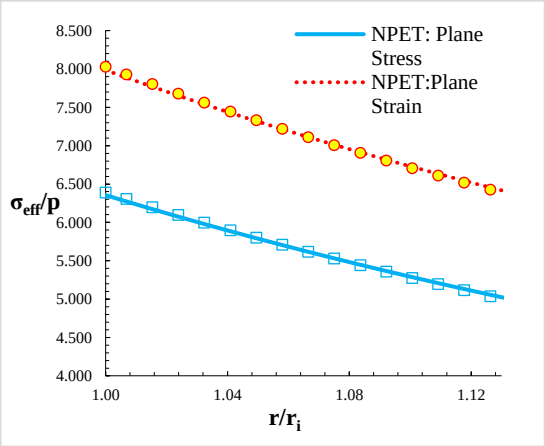

Fig. 11. Distribution of von Mises effective stress calculated by NPET and PET, $P_i = 8$ MPa (homogeneous cylinder)

Figure 11 shows the distribution of von Mises effective stress, for plane strain and plane stress conditions. It is observed that the values of von Mises effective stress at the inner layer of the cylinder for NPET is lower than PET results and at the outer layer of the cylinder it is higher than PET results.

4.2.2. Effects of Thickness

The cylinder thickness is another parameter that affects its nonlinear behavior. So, the displacement of cylindrical shells subjected to internal pressure $P_i^* = 0.0914$ for different thicknesses is studied. Results are shown in Figures 12 to 15. For these figures, the middle surface radius is $R = 40$ mm and the inhomogeneity constant is $n = 0$.

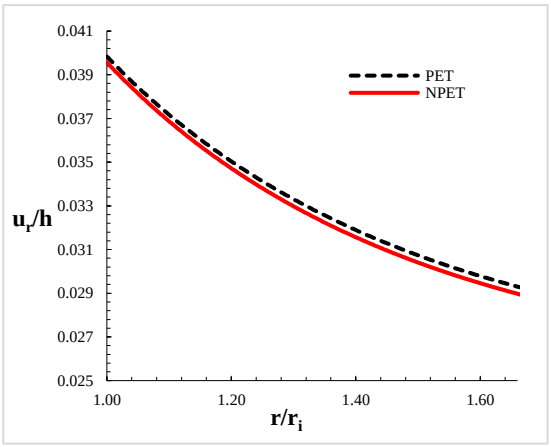

Fig. 12. Distribution of dimensionless radial displacement for $h = 20$ mm

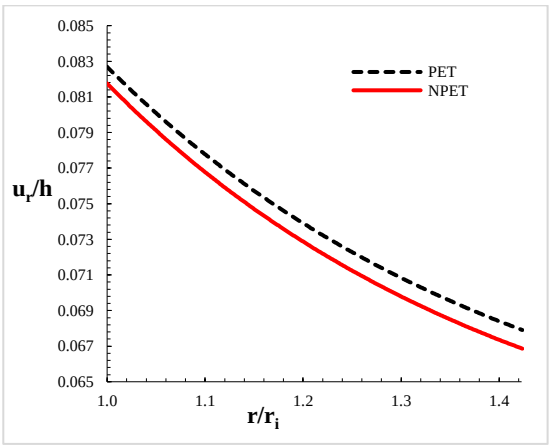

Fig. 13. Distribution of dimensionless radial displacement for $h = 14$ mm

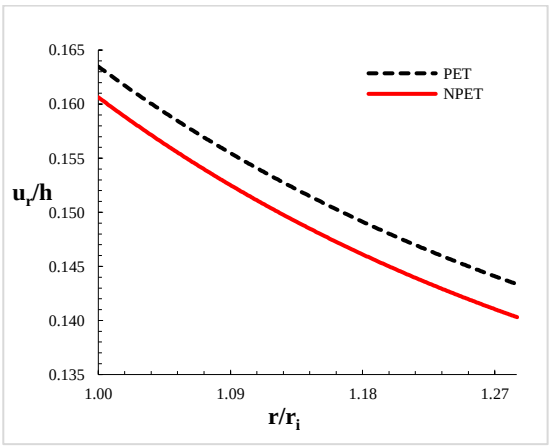

Fig. 14. Distribution of dimensionless radial displacement for $h = 10$ mm

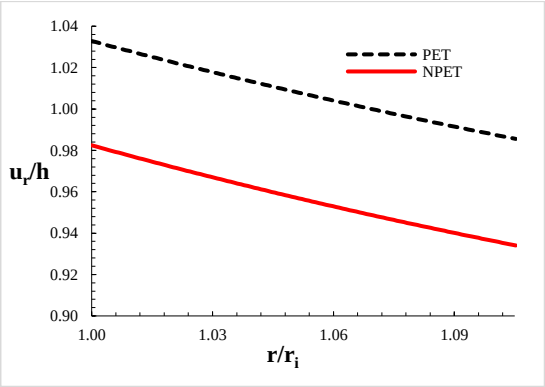

Fig. 15. Distribution of dimensionless radial displacement for $h = 4$ mm

By reducing the thickness, cylinder can no be assumed a thick wall cylinder, therefore, as shown in Figures 12 to 15, thickness reduction causes significant difference in linear and non-linear radial displacement.

4.2.3. Effects of Pressure and Young's Modulus

To show the effects of the loading and material parameters on the nonlinear response, the distribution of the displacement of the cylindrical shell for four amounts of pressure $P_o^* = 0.04, 0.0914, 0.0032, 0.00914$ are plotted in Figures 16 to 19. For all figures in this section, $r_i = 30$ mm, $r_o = 34$ mm, $n = 0$, $\nu = 0.3$.

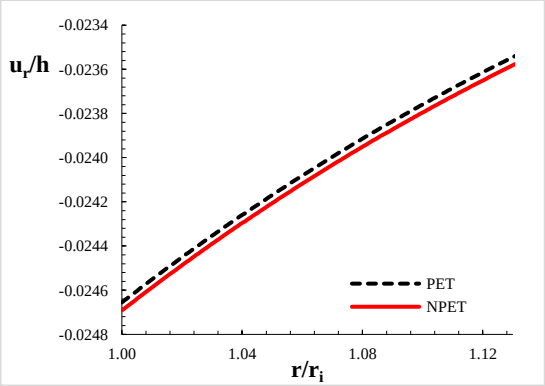

Fig. 16. Distribution of dimensionless radial displacement for $P_o^* = 0.0032$

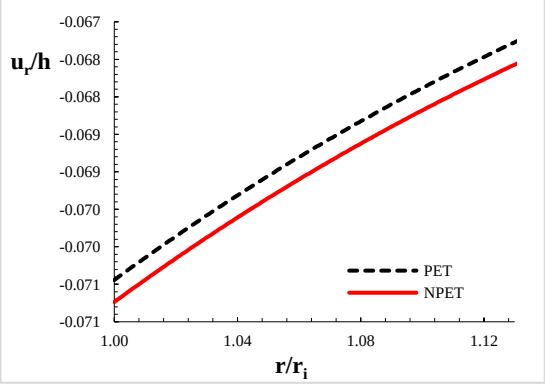

Fig. 17. Distribution of dimensionless radial displacement for $P_o^* = 0.00914$

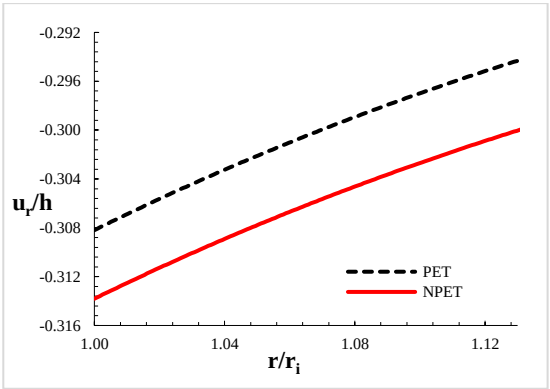

Fig. 18. Distribution of dimensionless radial displacement for $P_o^* = 0.04$

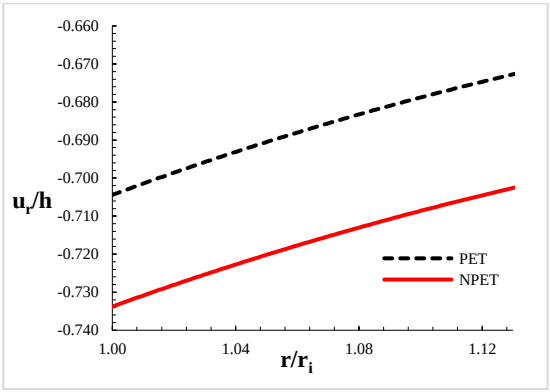

Fig. 19. Distribution of dimensionless radial displacement for $P_o^* = 0.0914$

Due to the dimensionless parameters:

$$P_o^* = \frac{P_o}{\epsilon E} = \frac{RP_o}{hE} \tag{25}$$

If the average radius (R), external pressure (P_o) and elasticity coefficient (E) be constant, thickness (h) and dimensionless pressure P_o^* will have an inverse relationship. According to Figures 16 to 19 during to increasing pressure (similar to decreasing thickness), the difference between linear and non-linear displacement increase.

4.3. Comparison with Numerical Solution Results

To compare the results with the Finite Element solution, a cylinder with inner radius $r_i = 30$ mm, outer radius $r_o = 34$ mm, length $L = 400$ mm and power distribution of modulus elasticity are considered. The modulus of elasticity at the inner surface is $E_i = 0.7$ GPa and the Poisson's ratio has a constant value of 0.3. This cylinder is subjected to equal internal and external pressures $P_i = P_o = 8$ MPa in plane strain state. The modeling is performed using ABAQUS software. According to the axisymmetric structure, CAX8R solid elements which have eight-node in the form of quadrilateral with curved sides are used for the modeling. In this type of element in addition to corner nodes, there are mid-

side nodes that enable to use nonlinear shape function (quadratic) for interpolation. The stiffness matrix for this element is 16∗16. The nonlinear behavior of cylinder is investigated by modeling the longitudinal section of pressurized shell.

In Figures 20 to 22, analytical solution is compared with the numerical solution. It is observed that the two solutions show good agreement.

In Table (1), the values of effective stress are given resulting from the analysis of the cylinder using NPET and PET for plane strain conditions under internal and external pressure at the inner, middle and outer layers. It is observed that for material with $n > 0$ ($n < 0$) the highest amount of effective stress occurs at the outer (inner) layer of the cylinder. The values of effective stress from FE analysis for $n > 0$ ($n < 0$) are more (less) than the values of effective stress from NPET solution.

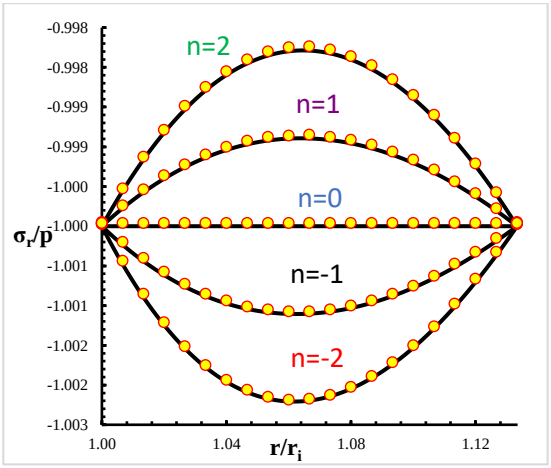

Fig. 21. Distribution of dimensionless radial stress calculated by NPET and FE, $P_i = P_o = 8$ MPa, (Plane strain state in nonhomogeneous cylinder)

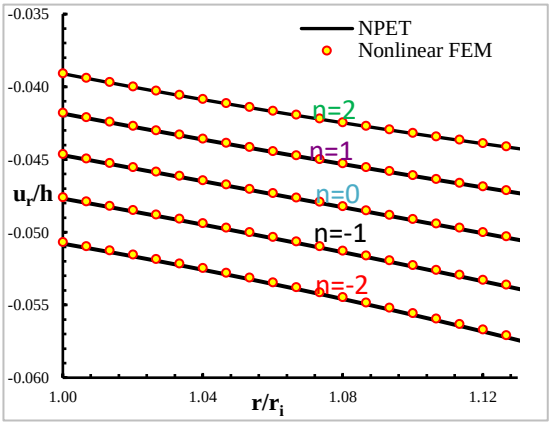

Fig. 20. Distribution of dimensionless radial displacement calculated by NPET and FE, $P_i = P_o = 8$ MPa, (Plane strain state in nonhomogeneous cylinder)

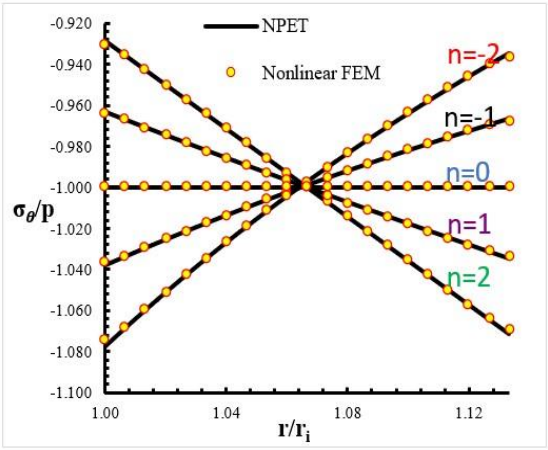

Fig. 22. Distribution of dimensionless circumferential stress calculated by NPET and FE, $P_i = P_o = 8$ MPa, (Plane strain state in nonhomogeneous cylinder)

Table 1. Distribution of von Mises effective stress [MPa] calculated by NPET and FEM, $P_i = P_o = 8$ MPa, (Plane strain state in nonhomogeneous cylinder)

$P_i = P_o = 8$ MPa	Solution	$n = -2$	$n = -1$	$n = 0$	$n = 1$	$n = 2$
Inner layer	NPET	0.420887	0.408928	0.4	0.39397	0.390641
	FEM	0.419987	0.408577	0.40	0.39411	0.39076
Middle layer	NPET	0.39988	0.400009	0.4	0.399842	0.399531
	FEM	0.39986	0.399987	0.40	0.399840	0.39954
Outer layer	NPET	0.391037	0.394374	0.4	0.408092	0.418783
	FEM	0.391140	0.394480	0.40	0.407818	0.418091

5. Conclusions

It can be concluded that positive (negative) values of n, make the shell more rigid (softer). So, as expected displacement in nonhomogeneous shells with $n < 0$ ($n > 0$) is more (less) than in homogeneous shells. Moreover, for $n > 0$ ($n < 0$) the highest amount of the value of the effective stress occurs in the outer (inner) layer. At the inner layer of shells the strength decrease (increase) for negative (positive) n compared to the homogenous shell.

The distribution of displacement in different ending conditions has significant differences. For plane strain condition it is more than plane stress condition. But it does not have significant differences for stresses. The lower (higher) the thickness of the shell, the more (the less) the difference between linear and nonlinear solutions. The softer (more rigid) material of the shell increases (decreases) this difference. Actually, for industrial applications in which materials are used with high Young's modulus, provided that the shell is not thin, shell behavior is highly linear and there is no need to study nonlinear behavior. So, in pressurized cylindrical shells, the nonlinear behavior can be seen in thin shells made of soft materials.

Funding Statement

This research did not receive any specific grant from funding agencies in the public, commercial, or not-for-profit sectors.

Conflicts of Interest

The author declares that there is no conflict of interest regarding the publication of this article.

Appendix

A.1. Dimensionless Parameters

$$u_r^* = \frac{u_r}{h}, \qquad r^* = \frac{r}{R}, \qquad \epsilon = \frac{h}{R} \ll 1, \qquad P_i^* = \frac{P_i}{\epsilon E}, \qquad P_o^* = \frac{P_o}{\epsilon E},$$
$$\frac{d}{dr} = \frac{1}{R}\frac{d}{dr^*}, \qquad \frac{d^2}{dr^2} = \frac{1}{R^2}\frac{d^2}{dr^{*2}} \tag{A1}$$

A.2. Equations

$$\begin{aligned}\sigma_r^* = (\bar{r})^n \Bigg[& \Big((At_1 + B)C_1 r^{*(t_1-1)} + (At_2 + B)C_2 r^{*(t_2-1)}\Big) \\ & + \epsilon \Bigg[\Big((At_1 + B)C_3\Big) r^{*(t_1-1)} + \Big((At_2 + B)C_4\Big) r^{*(t_2-1)} \\ & + \left(\left(\frac{1}{(2t_1 - t_2 + 1)} - \frac{1}{(t_1 + 1)}\right)\frac{(A(2t_1 + 1) + B)K_1}{(t_2 - t_1)}\right) r^{*(2t_1)} \\ & + \left(\left(\left(\frac{1}{(t_2 + 1)} - \frac{1}{(2t_2 - t_1 + 1)}\right)\frac{(A(2t_2 + 1) + B)K_2}{(t_2 - t_1)}\right)\right) r^{*(2t_2)} \\ & + \left(\left(\frac{1}{(t_1 + 1)} - \frac{1}{(t_2 + 1)}\right)\frac{(A(t_1 + t_2 + 1) + B)K_3}{(t_2 - t_1)}\right) r^{*(t_1+t_2)} \\ & + \left(\frac{(At_1{}^2 + B)}{2} C_1^2\right) r^{*2(t_1-1)} + \left(\frac{(At_2{}^2 + B)}{2} C_2^2\right) r^{*2(t_2-1)} \\ & + \Big((At_1t_2 + B)C_1C_2\Big) r^{*(t_1+t_2-2)} \Bigg] \Bigg] \end{aligned} \tag{A2}$$

$$C_1 = \frac{\left(\frac{P_o^*}{k^n} - P_i^* k^{(t_2-1)}\right)}{(At_1 + B)(k^{(t_2-1)} - k^{(t_1-1)}) r_i^{*(t_1-1)}} \tag{A3}$$

$$C_2 = \frac{\left(P_i^* k^{(t_1-1)} - \frac{P_o^*}{k^n}\right)}{(At_2 + B)(k^{(t_2-1)} - k^{(t_1-1)}) r_i^{*(t_2-1)}} \tag{A4}$$

$$\begin{aligned} C_3 = {} & \frac{-(A(2t_1+1)+B)\left(\frac{1}{(2t_1-t_2+1)} - \frac{1}{(t_1+1)}\right) K_1\left(k^{(t_2-1)} r_i^{*2t_1} - r_o^{*2t_1}\right)}{(At_1+B)(t_2-t_1)(k^{(t_2-1)} - k^{(t_1-1)}) r_i^{(t_1-1)}} \\ & + \frac{-(A(2t_2+1)+B)\left(\frac{1}{(t_2+1)} - \frac{1}{(2t_2-t_1+1)}\right) K_2\left(k^{(t_2-1)} r_i^{*2t_2} - r_o^{*2t_2}\right)}{(At_1+B)(t_2-t_1)(k^{(t_2-1)} - k^{(t_1-1)}) r_i^{(t_1-1)}} \\ & + \frac{-(A(t_1+t_2+1)+B)\left(\frac{1}{(t_1+1)} - \frac{1}{(t_2+1)}\right) K_3\left(k^{(t_2-1)} r_i^{*(t_1+t_2)} - r_o^{*(t_1+t_2)}\right)}{(At_1+B)(t_2-t_1)(k^{(t_2-1)} - k^{(t_1-1)}) r_i^{(t_1-1)}} \\ & + \frac{-\frac{1}{2}(At_1^2+B)\left(k^{(t_2-1)} r_i^{*2(t_1-1)} - r_o^{*2(t_1-1)}\right)}{(At_1+B)(k^{(t_2-1)} - k^{(t_1-1)}) r_i^{(t_1-1)}} C_1^2 \\ & + \frac{-\frac{1}{2}(At_2^2+B)\left(k^{(t_2-1)} r_i^{*2(t_2-1)} - r_o^{*2(t_2-1)}\right)}{(At_1+B)(k^{(t_2-1)} - k^{(t_1-1)}) r_i^{(t_1-1)}} C_2^2 \\ & + \frac{-(At_1t_2+B)\left(k^{(t_2-1)} r_i^{*(t_1+t_2-2)} - r_o^{*(t_1+t_2-2)}\right)}{(At_1+B)(k^{(t_2-1)} - k^{(t_1-1)}) r_i^{(t_1-1)}} C_1 C_2 \end{aligned} \tag{A5}$$

$$\begin{aligned} C_4 = {} & \frac{(A(2t_1+1)+B)\left(\frac{1}{(2t_1-t_2+1)} - \frac{1}{(t_1+1)}\right) K_1\left(k^{(t_1-1)} r_i^{*2t_1} - r_o^{*2t_1}\right)}{(At_2+B)(t_2-t_1)(k^{(t_2-1)} - k^{(t_1-1)}) r_i^{(t_2-1)}} \\ & + \frac{(A(2t_2+1)+B)\left(\frac{1}{(t_2+1)} - \frac{1}{(2t_2-t_1+1)}\right) K_2\left(k^{(t_1-1)} r_i^{*2t_2} - r_o^{*2t_2}\right)}{(At_2+B)(t_2-t_1)(k^{(t_2-1)} - k^{(t_1-1)}) r_i^{(t_2-1)}} \\ & + \frac{(A(t_1+t_2+1)+B)\left(\frac{1}{(t_1+1)} - \frac{1}{(t_2+1)}\right) K_3\left(k^{(t_1-1)} r_i^{*(t_1+t_2)} - r_o^{*(t_1+t_2)}\right)}{(At_2+B)(t_2-t_1)(k^{(t_2-1)} - k^{(t_1-1)}) r_i^{(t_2-1)}} \\ & + \frac{\frac{1}{2}(At_1^2+B)\left(k^{(t_1-1)} r_i^{*2(t_1-1)} - r_o^{*2(t_1-1)}\right)}{(At_2+B)(k^{(t_2-1)} - k^{(t_1-1)}) r_i^{(t_2-1)}} C_1^2 \\ & + \frac{\frac{1}{2}(At_2^2+B)\left(k^{(t_1-1)} r_i^{*2(t_2-1)} - r_o^{*2(t_2-1)}\right)}{(At_2+B)(k^{(t_2-1)} - k^{(t_1-1)}) r_i^{(t_2-1)}} C_2^2 \\ & + \frac{(At_1t_2+B)\left(k^{(t_1-1)} r_i^{*(t_1+t_2-2)} - r_o^{*(t_1+t_2-2)}\right)}{(At_2+B)(k^{(t_2-1)} - k^{(t_1-1)}) r_i^{(t_2-1)}} C_1 C_2 \end{aligned} \tag{A6}$$

References

[1] Truesdell, C., 1984. Mechanics of solids, vol. II: Linear theories of elasticity and thermoelasticity. Springer-Verlag, Berlin.

[2] Shi Z., Zhang T. and Xiang H., 2007. Exact solutions of heterogeneous elastic hollow cylinders. *Composite Structures*, 79(1), pp. 140-147.

[3] Sanders J., 1963. Nonlinear theories for thin shells. *Quarterly of Applied Mathematics, 21*(1), pp. 21-36.

[4] Fukui Y. and Yamanaka N., 1992. Elastic analysis for thick-walled tubes of FGM subjected to internal pressure. *Journal of JSME. Ser. 1, Solid Mechanics; Strength of Materials, 35*(4), pp. 379-385.

[5] Hughes T.J. and Liu W.K., 1981. Nonlinear finite element analysis of shells: part I. Three-dimensional shells. *Computer Methods in Applied Mechanics and Engineering, 26*(3), pp. 331-362.

[6] Ghannad M. and Nejad M.Z., 2012. Complete elastic solution of pressurized thick cylindrical shells made of heterogeneous FGM. *Mechanika, 18*(6), pp. 640-649.

[7] Ghannad M. and Gharooni H., 2012. Displacements and stresses in pressurized thick FGM cylinders with varying properties of power function based on HSDT. *Journal of Solid Mechanics, 4*(3), pp. 237-251.

[8] Ghannad M. and Nejad M.Z., 2012. Elastic analysis of heterogeneous thick cylinders subjected to internal or external pressure using shear deformation theory. *Acta Polytechnica Hungarica, 9*(6), pp. 117-136.

[9] Ghannad M., Rahimi G.H. and Nejad M.Z., 2013. Elastic analysis of pressurized thick cylindrical shells with variable thickness made of functionally graded materials. *Composites Part B: Engineering, 45*(1), pp. 388-396.

[10] Bich D.H. and Van Tung H., 2011. Non-linear axisymmetric response of functionally graded shallow spherical shells under uniform external pressure including temperature effects. *Journal of Non-Linear Mechanics, 46*(9), pp. 1195-1204.

[11] Duc N.D., 2014. Nonlinear static and dynamic stability of functionally graded plates and shells. Vietnam National University Press, Hanoi, Vietnam.

[12] Anh V.T.T., Bich D.H. and Duc N.D., 2015. Non-linear stability analysis of thin FGM annular spherical shells on elastic foundations under external pressure and thermal loads. *European Journal of Mechanics A/Solids, 50*, pp. 28-38.

[13] Kar V. and Panda S.K., 2016. Nonlinear thermomechanical deformation behavior of P-FGM shallow spherical shell panel. *Chinese Journal of Aeronautics, 29*(1), pp. 173-183.

[14] Srividhya S., Raghu P., Rajagopal A. and Reddy J.N., 2018. Nonlocal nonlinear analysis of functionally graded plates using third-order shear deformation theory. *International Journal of Engineering Science, 125*, pp. 1-22.

[15] Sofiyev A.H. and Dikmen F., 2020. Buckling analysis of functionally graded shells under mixed boundary conditions subjected to uniform lateral pressure. *Journal of Applied and Computational Mechanics, 7*(1), pp. 345-354.

[16] Quan T.Q, Ha D.T.T. and Duc N.D., 2022. Analytical solutions for nonlinear vibration of porous functionally graded sandwich plate subjected to blast loading. *Thin-Walled Structures, 170,* 108606.

[17] Bahadorani N., Ghannad M. and Sohani M.H., 2024. Complete solution of pressurized thick cylinders with large deformation using nonlinear plane elasticity theory. *Mechanical Engineering Journal of Tabriz University, 53*(3), pp. 163-171, (In Persian).

[18] Ellouz H., Jrad H., Wali M. and Dammak F., 2023. Numerical modeling of geometrically nonlinear responses of smart magneto-electro-elastic functionally graded double curved shallow shells based on improved FSDT. *Computers and Mathematics with Applications, 151*, pp. 271-287.